Chain Packing in Ethylene−Butene Copolymers

Arun Neelakantan, Rory Stine, and Janna K. Maranas*

Department of Chemical Engineering, The Pennsylvania State University, University Park, Pennsylvania 16802

Received July 8, 2002

ABSTRACT: We investigate intermolecular packing in a series of five ethylene/butene random copolymers and various binary mixtures of the pure components using molecular dynamics simulation. The simulation model provides chain dimensions and solubility parameters as a function of butene content that are consistent with experiment. In pure materials, intermolecular packing varies directly with butene content, with low butene content materials packing more efficiently. If butene placement is made alternating instead of random, the material behaves as if its butene content has been lowered. In mixtures, the dominant trend is for the more efficient packer to increase its self-packing, while the less efficient packer decreases its self-packing—in other words, the two distributions move further apart on mixing. In these cases, the cross-correlation is described by an average of the two components. In some instances, large preferences for cross-correlations are observed at the expense of self-correlations. In addition, an efficient packer is more resistant to changes of self-packing on mixing than a poor packer, and self-packing changes more if the material is placed in a dissimilar environment.

I. Introduction

Chain packing refers to the extent of ordering between different chains in the melt. This can be characterized by the intermolecular pair distribution function, which measures the local density of intermolecular contacts relative to the bulk density as a function of separation. Within the series of saturated hydrocarbon polymers, this ordering varies with respect to both the strength of the ordering, indicated by the height of the nearest-neighbor peak in $g^{\text{inter}}(r)$, and the spatial location of this peak.[1] This ordering affects both thermodynamic and dynamic properties, for example the cohesive energy density,[2] and local mobility.[3] This paper investigates a series of copolymers made of ethylene and butene units placed randomly along the chain. Within this series, the extent of ordering varies, but the spatial location of the peak does not. These materials have been extensively characterized by Krishnamoorti,[4−8] who reported chain dimensions and cohesive energy densities as a function of butene content. When blended, they form the majority of the cases in which "regular" mixing is observed,[1,7,9] meaning that the Flory interaction parameter is proportional to the difference in pure component solubility parameters.[10]

Here we are interested in intermolecular packing of these materials and how this packing varies with mixing, all of which are difficult to isolate experimentally, and thus we use molecular dynamics simulations to investigate the changes in packing with butene content. We first test the ability of the simulation model to describe these materials by comparing the cohesive energy density and chain dimensions with experimental results. Having found that the model describes the changes in both with butene content in a reasonable manner, we characterize intermolecular packing in pure materials. Last, we consider how molecular packing changes when a material is mixed with various second components.

II. Background

Packing in Polymer Melts. Intermolecular packing in polyolefin melts has been investigated using computer simulation[1,2,11−16] and the liquid state theory PRISM.[17−21] Both methods show that although intermolecular packing in polyolefins is universal on length scales of R_g and greater, at short distances, intermolecular packing varies significantly as a function of pendant group spacing and size. The most important factor is the pendant group spacing. If the spacing is low as in isotactic polypropylene [iPP], preferential packing of chains is prevented, whereas packing is enhanced as pendant groups become more spread out as in polyethylene [PE].[1] The location of the closest packing distance is also affected, as alluded to in the Introduction. A secondary factor is the pendant group size. Packing is decreased as the size of the pendant group is increased, but the size of the effect is much smaller than that of pendant group spacing.[1] In addition to the molecular dynamics results described above, these trends have been observed in a systematic study of pendant group spacing and size using PRISM.[21]

Here we extend our previous observations to randomly sequenced copolymers. We find that packing scales directly with the composition of butene units: the less butene present, the more efficient intermolecular packing becomes. As with our study of homopolymers, the cohesive energy densities of the copolymers also increase with intermolecular packing. We also compare a random copolymer of 67% butene with poly(ethylene−butene) (PEB), an alternating polymer with the same butene branch content. We find that randomizing the branches increases their effect; i.e., an alternating material packs more efficiently than a random material with the same butene content.

Packing in Polymer Blends. In an A−B blend, there are three relevant distributions: A/A, B/B, and A/B. The mixture results we present here are concerned with the changes in the A/A and B/B distributions from the melt state, in various second components B or A. We also consider the A/B distribution. Studies of packing in mixtures have been done using PRISM calculations with the semiflexible chain model on athermal (purely repulsive),[22−24] symmetric (energetic interactions of the two components are equal),[25] and asym-

10.1021/ma0210729 CCC: $25.00
Published on Web 04/18/2003

metric blends.[26] In athermal blends, the component with the most ordering, or the stiffer component, becomes more ordered on mixing, while that which packs least efficiently in the melt becomes even less ordered; i.e., the two distributions move further apart. The cross-correlation A/B closely follows either the geometric or arithmetic combining rules. In symmetric blends (i.e., equivalent A−A and B−B interactions) with favorable A−B interactions the cross-correlation is enhanced at the expense of like correlations. For asymmetric blends, the stiffer or better-packing component packs less efficiently and the more flexible component packs more efficiently (i.e., the two distributions move closer together) on mixing. The A/B distribution shows a preference for clustering of like, rather than unlike, monomers. This work has clearly demonstrated the importance of local and nonuniversal packing distributions on miscibility of polymer blends, particularly with respect to the polyolefins.[27]

Blends of polyolefins that have been specifically addressed include PE/hhPP,[28] polypropylenes of varying tacticities (sPP/iPP, iPP/aPP, and aPP/sPP),[29] and PE/iPP.[30] The PE/hhPP blend, which was investigated using Monte Carlo (MC) simulation on a high coordination lattice, is immiscible, with both the PE/PE and hhPP/hhPP distributions showing like species clustering. The polypropylene blends have been addressed via both MC simulation and PRISM. MC results for iPP/aPP reveal little change in either of the intermolecular distributions, whereas both iPP/sPP and aPP/sPP have enchanced self-packing and low A/B correlation with the effect larger for iPP/sPP. This is again consistent with immiscibility. The PRISM results for iPP/sPP, which are for much shorter chain lengths ($N = 12$ vs $N = 150$), do not show like species clustering and instead reveal little change in like species distributions, suggesting a miscible system. The PE/iPP blend is also generally accepted as strongly immiscible. The PRISM results for this system show clustering of PE in the blend relative to the pure melt, with the effect increasing at extreme compositions.

Our results include 10 blends formed from five copolymers which, at the chain lengths studied experimentally, range from immiscible to those whose mixing follows the solubility parameter formalism.[4,7,9,31] We follow the changes in each material as is it mixed with the other four, thus revealing the effect of each copolymers environment on its intermolecular packing. At the chain lengths in our simulations, all of the mixtures are miscible, with some having significant clustering of unlike species. We find three general trends: (1) In a mixture of a "good" packer with a "poor" packer, the material that packs well tends to pack even better, while the poor packer packs even less efficiently. This trend follows the athermal PRISM results. The blends of H71−H65 and H47−H65 do not obey this trend but rather have significant A−B clustering. (2) A material that packs well is more resistant to altering that packing when mixed. (3) Blends where the pure components have similar packing efficiencies change less than those with vastly different packing efficiencies.

III. Simulation Methods

A. Model. The model is an extension of the optimized force field for liquid hydrocarbons (OPLS) introduced by Jorgensen et al.[32] The united atom method is used, which represents the molecules as a series of carbon containing groups such as C, CH, CH_2, and CH_3. Covalent bonds are represented by constraint forces on each united atom, maintaining a fixed carbon−carbon bond length of 1.54 Å. Bonded interactions are taken into account through bending and torsional potentials, while nonbonded interactions are characterized by Lennard-Jones (LJ) interaction sites located at the center of mass of each united atom. A full discussion of the model can be found in ref 2. The equations of motion were integrated by means of the standard velocity Verlet algorithm[33] using a time step of 5 fs, and the bond length was kept constant using the RATTLE algorithm.[33]

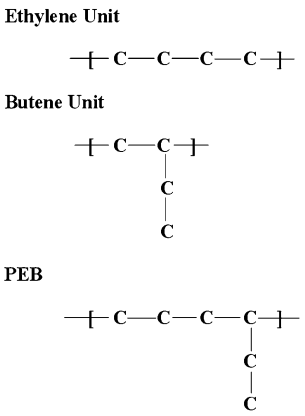

Figure 1. Structure of the monomer units in EB copolymers and in PEB. The hydrogens are omitted for clarity.

The initial configurations for all the systems considered in this study were generated as described by Mondello et al.[33] The chain is first generated in an all-trans configuration. Multiple copies of this chain are then placed in a cubic MD cell whose size is sufficiently large to ensure that none of the chains overlap. The MD program is then run to allow the chains to relax, and at the same time the box size is gradually reduced to the desired value (governed by the density of the material). This phase of the relaxation process is carried out over 200 ps. The torsional energy was initially zero (all trans) and rose quickly, requiring ∼40 ps to stabilize at a relevant trans/gauche value. Thus, the conformation quickly loses memory of the imposed initial state.

Randomized ethylene−butene copolymer molecules, with a fixed percentage of butene monomers per chain, were generated as described below. A molecular size of 62 united atoms was selected to allow the molecules to be truly randomized while still minimizing computing time. The structure of each monomer unit is given in Figure 1. An ethylene unit is represented as a linear chain of four carbon atoms, and a butene unit is a branched chain of four carbon atoms. Since the sizes of both the units are equal, every molecule will consist of a total of 16 units irrespective of the butene content. To create each random copolymer, a random number from 1 to n ($n = X + Y$; X = number of ethylene units, Y = number of butene units) is generated. If the random number is less than X, an ethylene unit is added to the molecule; if not, a butene unit is added. The number of X or Y units remaining is then updated. This process is repeated until the entire chain is generated. All chains are generated individually using this algorithm. Systems with butene compositions of 17, 30, 47, 65, and 71% (designated H17, H30, H47, H65, and H71, respectively) were generated to give a range of components

Table 1. Densities of C62 EB Copolymers

material	density (g/cm^3)	material	density (g/cm^3)
H17	0.7528	H65	0.7628
H30	0.7553	H71	0.7640
H47	0.7590		

spanning pure polyethylene (PE) to pure polybutene (PB).

All simulations were run with a system of 50 molecules and at a temperature of 150 °C. A constant temperature was maintained during each simulation using the velocity rescaling algorithm of Berendsen et al.[34] To perform the simulations, we require the oligomer densities for each copolymer. Since the experimental oligomer densities for copolymers are not available, they were estimated by scaling the experimental polymer densities as follows:

$$\rho^i_{C62} = \rho^i_{polymer}\left(\frac{\rho^{PE}_{C62}}{\rho^{PE}_{polymer}}\right) \quad (1)$$

ρ^{PE}_{C62} (i.e., *h*00) was obtained from ref 34, and $\rho^{PE}_{polymer}$ was obtained from ref 31. The $\rho^i_{polymer}$ were obtained by linear regression of experimental ethylene−butene copolymer densities at 150 °C as a function of butene content. The resulting densities ρ^i_{C62} used in the simulation are given in Table 1. All blends have 25 chains of A and 25 chains of B. The blend density is calculated from pure component densities assuming no volume changes on mixing. Experimental results show this is a good approximation for these systems.[35]

B. Calculated Quantities. Cohesive Energy Density and Internal Pressure. The cohesive energy density (CED) is defined as the energy of vaporization per unit volume:

$$\Pi_{CED} = \frac{U_L - U_G}{V} = \frac{U_{inter}}{V} \quad (2)$$

Here we approximate the energy of vaporization with the intermolecular energy as shown in the second equality. The internal pressure is defined as the derivative of internal energy with respect to volume:

$$\Pi_{IP} = \left(\frac{\partial U_L}{\partial V}\right)_{T,N} \quad (3)$$

We calculate the internal pressure by varying the system volume while holding the number of chains and the temperature of the system constant and plotting the resulting internal energy vs volume. The slopes of these plots, an example of which is shown in Figure 2, give the internal pressure. For CED calculations and determinations of internal energy to assess internal pressure, an equilibration run of 1 ns was performed first, followed by a data acquisition run of 1 ns, with data dumps occurring in 2.5 ps intervals.

Pair Distribution Functions. The pair distribution functions are defined as

$$[g(r)]_{inter} = \frac{\langle \rho(r')[\rho(r'+r)]_{inter}\rangle}{\langle \rho(r')_{inter}\rangle^2} \quad (4)$$

$$[g(r)]_{intra} = \frac{\langle \rho(r')[\rho(r'+r)]_{intra}\rangle}{\langle \rho(r')_{intra}\rangle^2} \quad (5)$$

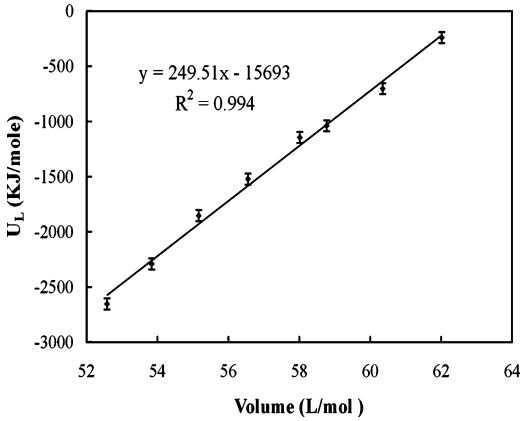

Figure 2. Illustrative plot of U_L vs volume for H71. The slope of the plot gives the internal pressure.

in which $\rho(r')$ and $\rho(r'+r)$ are the instantaneous densities of united atoms at the locations r' and $r'+r$. The subscript "inter" in eq 4 means that only the pairs on different molecules are counted, and the subscript "intra" in eq 5 means that only the pairs on the same molecule are counted. The angular brackets indicate averages of all r' locations of united atoms in the simulation box, with $\langle\rho(r')\rangle$ equal to the macroscopic density.

The actual calculation of the pair distribution functions was implemented as described below. The numerator is determined from the simulation in the form of a histogram $H(r)$, which is normalized using a suitable normalization factor (NF). The choice of an appropriate normalization factor results in $g(r)$ approaching unity for large separation. Although this choice is obvious for the total distribution, for intermolecular distributions and A/A, B/B, and A/B distributions in mixtures the situation is less clear. This problem was addressed by Stevenson et al.[22] For the total distribution function, NF is the two-site probability of *uncorrelated* particles at positions r and r'. For the intermolecular pair distribution function, NF is the two site probability of uncorrelated particles on different chains at positions r and r'. The placement of one site at r leaves that chain and the volume occupied by that chain inaccessible for the second site. Thus, the normalization factor is given by

$$NF_{inter} = \frac{N}{V}\left(\frac{N-n}{V-v}\right) = \frac{N^2}{V^2}\left(\frac{1-1/m}{1-v/V}\right) \quad (6)$$

where N is the total number of united atoms, V is the volume of the box, n is the number of united atoms in a chain, m is the total number of chains, and v is the volume occupied by a single chain. Because the density is constant throughout the box, its volume can be expressed as $V = mv$ and NF_{inter} reduces to N^2/V^2.

Following the same reasoning, the normalization factor for $g_{AA}(r)$ in a mixture is

$$NF^{AA}_{inter} = \frac{N_A}{V}\left(\frac{N_A - n_A}{V - v_A}\right) = \frac{N_A{}^2}{V^2}\left(\frac{1-1/m_A}{1-v_A/V}\right) \quad (7)$$

due to the additional constraint that the uncorrelated particles must be of the same identity. Here N_A is the total number of A united atoms, n_A is the number of A united atoms on a single chain, m_A is the number of A chains, v_A is the volume occupied by an A chain, and

the total volume $V = m_A v_A + m_B v_B$. We would now like to replace the volume v_A in eq 7 with the mole fraction X_A. Although in the current work we consider only 50/50 blends, we begin with the general case of mole fractions X_A and X_B, where

$$X_A = \frac{N_A}{N_A + N_B} = \frac{m_A n_A}{m_A n_A + m_B n_B} \tag{8}$$

Since we assume equal volumes, $v_{A\ atom} = v_{B\ atom} = v_{atom}$, the volume fraction is proportional to the mole fraction:

$$\frac{v_A}{V} = \frac{v_{atom} n_A}{v_{atom}(m_A n_A + m_B n_B)} = \frac{n_A}{m_A n_A + m_B n_B} = \frac{X_A}{m_A} \tag{9}$$

Putting this back in eq 7 results in the following for the AA normalization factor:

$$\mathrm{NF}_{inter}^{AA} = \frac{{N_A}^2}{V^2}\left(\frac{1 - 1/m_A}{1 - X_A/m_A}\right) \tag{10}$$

A similar argument holds for $g_{BB}(r)$. For $g_{AB}(r)$ the normalization factor is given by

$$\mathrm{NF}_{inter}^{AB} = \frac{N_B}{V}\left(\frac{N_A}{V}\right) + \frac{N_A}{V}\left(\frac{N_B}{V}\right) = \frac{2N_A N_B}{V^2} = 2X_A X_B\left(\frac{N^2}{V^2}\right) \tag{11}$$

The normalization factors in eqs 10 and 11 are used with $X_A = X_B = 0.5$ when calculating A/A and A/B pair distribution functions.

Chain Dimensions. The radius of gyration is defined as

$$R_g = \langle|(\mathbf{r}_i - \mathbf{r}_{CM})|\rangle \tag{12}$$

where $\mathbf{r}_i$ is the position of atom i and $\mathbf{r}_{CM}$ is the position of the center of mass of the molecule that atom i belongs to.

The end-to-end distance is defined as

$$R_e = \langle|(\mathbf{r}_1 - \mathbf{r}_n)|\rangle \tag{13}$$

where $\mathbf{r}_1$ and $\mathbf{r}_n$ are the positions of the first and last atom of a chain.

Time-Dependent Functions. The mean-square displacement is defined as

$$\mathrm{msd}(t) = \langle|\mathbf{r}(t) - \mathbf{r}(0)|^2\rangle \tag{14}$$

where $\mathbf{r}(t)$ is the position of an atom at time t.

The energy autocorrelation function is defined as

$$E(t) = \frac{\langle(U(t_0) - \bar{U})(U(t + t_0) - \bar{U})\rangle}{\langle(U(t_0) - \bar{U})^2\rangle} \tag{15}$$

where $\bar{U}$ is the average internal energy of the system and $U(t_0)$ and $U(t_0+t)$ are the instantaneous values of the internal energy.

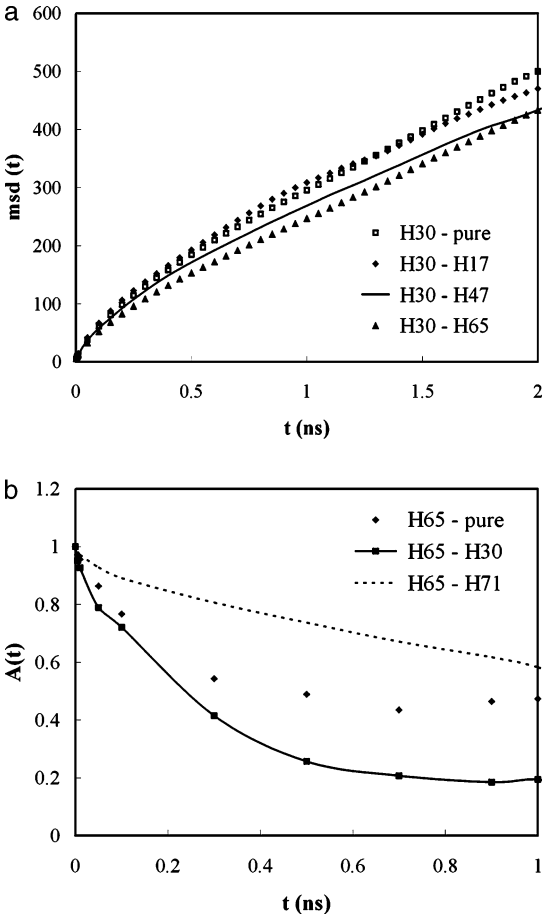

Figure 3. Functions used to assess equilibration: (a) mean-square displacement of united atoms, msd(t); (b) end-to-end vector autocorrelation function, $A(t)$. Symbols are as in figure legend.

Similarly, the end-to-end vector autocorrelation function is defined as

$$A(t) = \frac{\langle(\mathbf{R}_e(t_0) - \overline{\mathbf{R}_e})(\mathbf{R}_e(t + t_0) - \overline{\mathbf{R}_e})\rangle}{\langle(\mathbf{R}_e(t_0) - \overline{\mathbf{R}_e})^2\rangle} = \frac{\langle\mathbf{R}_e(t_0)\mathbf{R}_e(t + t_0)\rangle}{\langle\mathbf{R}_e(t_0)^2\rangle} \tag{16}$$

where $\mathbf{R}_e(t)$ is the instantaneous value of the end-to-end distance vector and $\overline{\mathbf{R}_e}$ is the average end-to-end vector. $\overline{\mathbf{R}_e}$ is equal to zero, and so the equation can be simplified as shown above.

IV. Equilibration

The criterion we use to assess equilibration in each system is that the mean distance moved by the united atoms is greater than $2R_g$. Equilibration times based on this criterion range from 1.5 to 2.5 ns. Mean-square displacements are shown in Figure 3a for pure H30 and H30 in H17, H47, and H65. The R_g for H30 (11 Å) does not change with mixing, and so the united atoms have moved between $1.8R_g$ (H30 in H65) and $2.0R_g$ (H30 pure) over the 2 ns time scale shown in the figure. We have also calculated the end-to-end vector autocorrelation functions. Example data, pure H65 and H65 in H30 and H71, are shown in Figure 3b. Data are shown up to 1 ns, beyond which the statistics become poor. The

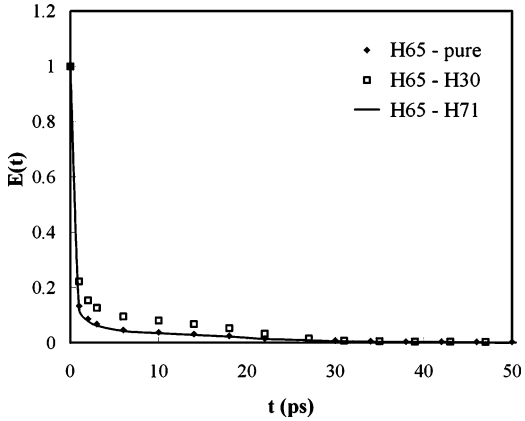

Figure 4. Total energy autocorrelation function, $E(t)$. Symbols are as in figure legend.

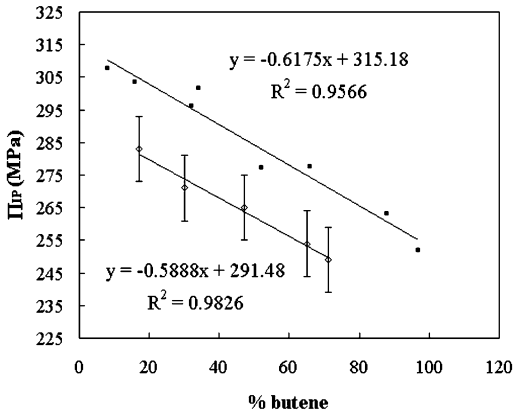

Figure 5. Comparison of internal pressures obtained from experiment and simulation as a function of butene content: filled squares, experimental results from ref 31; open diamonds, simulation results from present work.

Table 2. Cohesive Energy Density and Internal Pressure for the EB Copolymers[a]

material	Π_{CED} (MPa)	Π_{IP} (MPa)	a	$(1 - a)$
H17	235	283	0.83	0.17
H30	225	271	0.83	0.17
H47	214	265	0.81	0.19
H65	203	254	0.80	0.20
H71	194	249	0.78	0.22
PEB	208	277	0.75	0.25

[a] The standard deviations are ±2 MPa for CED and ±10 MPa for internal pressure.

Table 3. Radius of Gyration (R_g) and End-to-End Distance (R_e) of EB Copolymers and Blends (the Standard Deviation for Both Is ±1 Å)

material	R_g (Å)	R_e (Å)	material	R_g (Å)	R_e (Å)
H17 (pure)	12	27	H47 in H30	10	24
H17 in H71	11	24	H47 in H17	10	25
H17 in H65	12	26	H65 (pure)	9	23
H17 in H47	12	27	H65 in H71	8	21
H17 in H30	11	24	H65 in H47	8	20
H30 (pure)	11	26	H65 in H30	9	22
H30 in H71	11	25	H65 in H17	9	22
H30 in H65	11	27	H71 (pure)	9	20
H30 in H47	10	24	H71 in H65	8	20
H30 in H17	11	25	H71 in H47	8	19
H47 (pure)	10	24	H71 in H30	8	20
H47 in H71	10	23	H71 in H17	9	21
H47 in H65	10	22	PE[a] (pure)	11	31

[a] The simulation was run at 150 °C on a system of 50 chains of 50 united atoms each.

result of mixing can be seen to enhance the decay if the host is faster (H65 in H30) or to retard the decay if the host is slower (H65 in H71). In all cases, this function has decayed to 0.2 or less before data collection runs are started. The total energy autocorrelation function is plotted in Figure 4 for pure H65 and H65 in H30 and H71. This function decays to zero well before the assigned equilibration times. Similar results were observed for other systems.

Following equilibration, data acquisition runs of 1.5 ns were performed for all systems, with coordinate dumps occurring every 2.5 ps. The radial distribution functions were then calculated as averages over every 500 ps and monitored for drifts that may indicate further equilibration is necessary. No such drifts were detected. The distribution functions for mixtures have larger variations than the pure components. Since the equilibration criteria used for mixtures was identical to the pure components, the larger variations do not indicate that the mixtures are further from equilibrium, but rather result from concentration fluctuations present in mixtures, but not in pure components. Similar observations were made in ref 27.

V. Results and Discussion

Evaluation of Simulation Model. Table 2 gives the values of cohesive energy density and internal pressure obtained using the simulation model described above. The term "a" represents the ratio of cohesive energy density to internal pressure and is representative of the fraction of intermolecular contacts.[36] Cohesive energy density is not experimentally measurable for polymers, and so internal pressure is used to provide estimates of solubility parameters [i.e., $(\Pi_{CED})^{1/2}$]. The cohesive energy density of poly(ethylene-*alt*-butene) (PEB) is included to study alternating ethyl branch placement as a contrast to the random copolymers. The structure of the PEB monomer is given in Figure 1. The fraction of intramolecular contacts $(1 - a)$ increases with butene content. This follows because larger butene contents increase the amount of branching in the molecules, hence making intramolecular contact more likely.

Plotted in Figure 5 are the simulated and experimental[31] internal pressures as a function of butene content. The experimental data are for long chain polymers, whereas the simulations are for C62 oligomers. The plot shows that, while there is an offset due to differences in molecular size, the overall trend with composition is maintained in comparison to the experimental data. Our previous work has shown that a procedure that involves simulating chains of various molecular sizes and extrapolating results in quantitative agreement between simulation and experiment.[1] We have not done such an analysis here due to the large amount of computation time required.

The radius of gyration (R_g) and end-to-end distance (R_e) of all materials we study are given in Table 3. The values obtained for H00 (PE) are consistent with previous simulation studies of PE of similar size.[37−39] Note that for PE we use 50 united atoms, whereas for the copolymers we use 62. A comparison between the simulated and experimental chain dimensions is presented in Figure 6 where $\langle R_0 \rangle^2/M$ ($\langle R_0 \rangle^2 = 6R_g^2$, M = molecular weight) is plotted as a function of butene content for both the present simulations and the experiments of Krishnamoorti et al.[8] While there is a slight

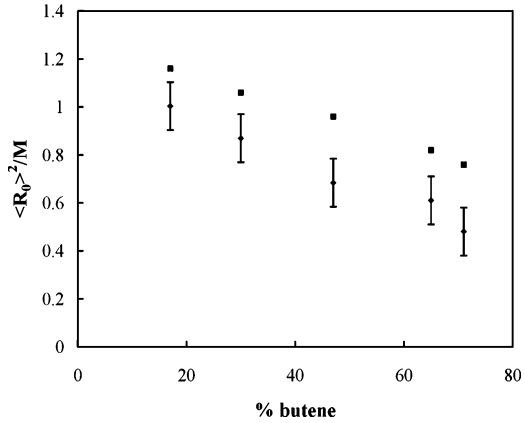

Figure 6. Comparison of experimental and simulated $\langle R_0 \rangle^2/M$ as a function of butene content: filled squares, experimental results from ref 31; open diamonds, simulation results from present work.

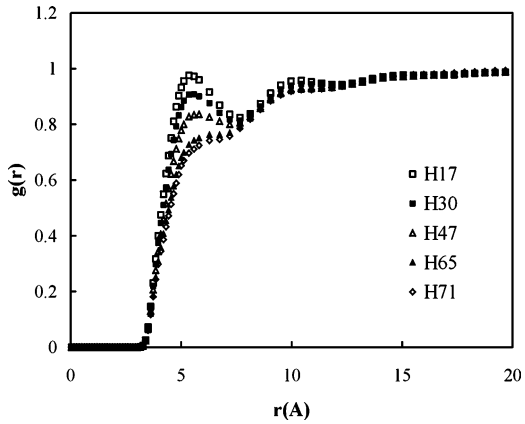

Figure 7. Intermolecular radial distribution function for EB copolymers with varying butene content. Symbols are as in figure legend.

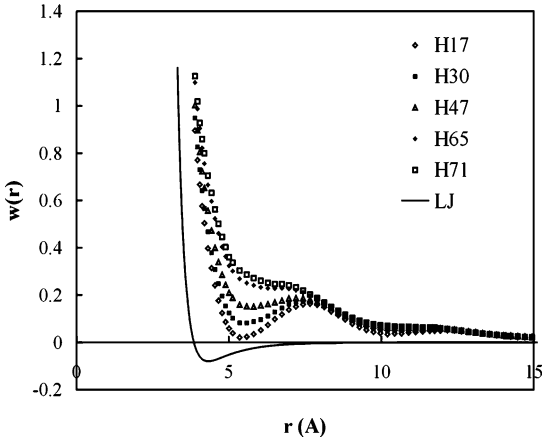

Figure 8. Potential of mean force of pure components compared to the Lennard-Jones potential. Symbols are as in figure legend.

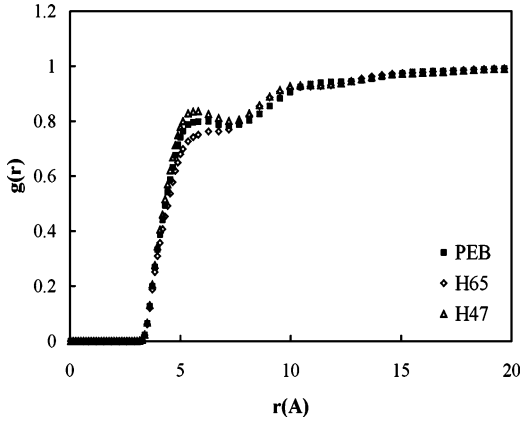

Figure 9. Intermolecular pair distribution functions of PEB, H65, and H47, illustrating the effect of randomizing branch location. Symbols are as in figure legend.

offset, the two curves show a similar trend with butene content.

Packing in Pure Components. Plotted in Figure 7 are the intermolecular pair distribution functions, $g(r)$, of the five pure components. As mentioned earlier, intermolecular packing becomes more efficient as the butene content is decreased. This is reflected in the peak centered around 5 Å becoming more pronounced at low butene contents such as H17. The R_g's of the higher butene content materials are around 8 Å, and beyond this distance, the distributions of high butene content materials show universal behavior, as expected. The lower butene content materials, with R_g's up to 12 Å, have a secondary peak located near $r = 10$ Å. At separations greater than 12 Å, all materials show universal behavior. As we have found in our previous work,[1] the cohesive energy densities of the random copolymers are greater for those materials with greater packing efficiency, as can been seen by comparing Table 2 with Figure 7.

Plotted in Figure 8 is the potential of mean force

$$\omega(r) = -kT \ln g(r)_{\text{inter}} \qquad (17)$$

for all materials. The potential of mean force represents the interaction of two united atoms held a distance r apart with the remaining united atoms averaged over all configurations. The advantage of this function is that it may be compared to the LJ potential, thus enabling one to assess the extent to which the potential is sampled in each system. Since the LJ potential itself would be obtained for an isolated pair of united atoms, the displacement between the potential of mean force and the LJ potential indicates the extent to which the surrounding united atoms affect the pair in question. Materials with more efficient packing have smaller such displacements so that the effects of the surrounding environment on pair separation are less. This is consistent with the molecular architecture of these materials—the more efficient packers have smaller branch contents and thus are less hindered in their configuration.

Alternating vs Random Branches. The strictly alternating PEB has the same branch content as the random material H65. A comparison of these materials thus affords the opportunity to ascertain the effect of randomizing branch placement. As can be seen in Figure 9, the $g(r)$ for PEB, rather than matching H65, lies between those of H65 and H47. A similar trend is apparent in the cohesive energy densities shown in Table 2. The implication is that if the random branches are made alternating (i.e., H65 → PEB) while maintaining the same branch concentration, the resulting material behaves as if its branch concentration has been lowered. Branches thus have a greater effect if they are randomized rather than alternating. The reason for this could be that if the branch placement is random, there will be some sequences with several consecutive butene

Table 4. Probability of Butene Sequences of Size *n* for PEB, H65, and H47

n	H65	H47	PEB
1	0.25	0.5	1
2	0.20	0.25	0
3	0.21	0.15	0
4	0.14	0.07	0
5	0.10	0.03	0
6	0.07	0	0
7	0.02	0	0
8	0	0	0
9	0.01	0	0
10	0	0	0

units, something which is not possible in an alternating material and that would be expected to have a significant effect on packing. To check this, we have calculated the distribution of butene groups in H65 and H47, and the results are given in Table 4. To obtain these data, we have located all sequences of consecutive butene groups among the molecules. The length of each sequence is tabulated, and the entries are normalized by the total number of sequences found. As it is alternating, butene in PEB may only occur as isolated units. In the random materials, approximately half [H47] and one-quarter [H65] of butene units are isolated. Sequences of up to five consecutive butene units have reasonable probabilities (10% or greater) of occurrence in H65, whereas H47 has similar probabilities only for sequences of three units or less.

Packing in Blends. We now consider the effects of blending on packing of these materials. We have formed mixtures from all combinations of the five materials: H17, H30, H47, H65, and H71. Not all of these pairs are miscible in their long chain versions or have been studied experimentally. Those that have been, H17−H30, H30−H47, H47−H65, and H65−H71, all have interaction parameters that are well described by the regular mixing prediction—they can be expressed in terms of pure component cohesive energy densities. We consider both the intra- and intermolecular pair distribution functions.

The intramolecular $g(r)$ is quite insensitive to blending as illustrated in Figure 10 for H17. Plotted in the figure are the intramolecular $g(r)$ curves for pure H17 and H17 in H30, H47, H65, and H71. Only a single curve is visible because all five curves coincide. Thus, no change in intramolecular structure occurs on mixing for H17. The other materials H30, H47, H65, and H71 show similar behavior. This suggests that intramolecular packing is a function of material only and is independent of its environment. We also note that chain dimensions—end-to-end distance and radius of gyration—do not change with environment, within the errors of our simulations.

The variation of intermolecular $g(r)$ with environment is illustrated in Figure 11. The figure shows A−A distributions of a given component in the melt and when blended with various second components B. The plot for H17 (Figure 11a) shows H17/H17 distributions in the melt and in blends with H30, H47, H65, and H71. In the figure legends, the component for which the calculation is being presented is written first, followed by the second component that forms the environment. For example, in Figure 11a the legend H17−H71 indicates the H17/H17 $g(r)$ calculated for the H17−H71 blend. In Figure 11e, the H71/H71 $g(r)$ for the same blend is indicated as H71−H17. It is obvious that, in contrast to its intramolecular counterpart, the intermolecular

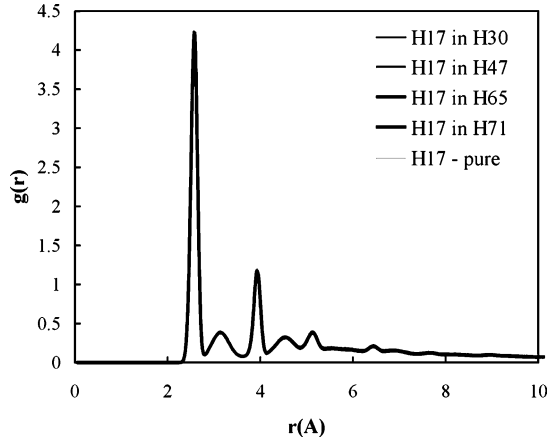

Figure 10. Intramolecular pair distribution function of H17 in different environments. Symbols are as in figure legend.

$g(r)$ can vary significantly as its environment is changed. We find three general trends: (1) In an A−B blend, the closer in structure B is to A, the less A tends to change on mixing. (2) A material that packs well is more resistant to altering that packing when mixed. (3) The direction of change is typically such that the efficient packers become even more efficient when mixed with poor packers and vice versa; i.e., the distributions move further apart on blending.

Trend 1 is best illustrated by the variation of H47 in Figure 11c. When blended with the materials closest in composition (and structure) to itself, H30 and H65 (note that these distributions lie on top of each other in the figure), the distribution is identical to the melt distribution, but when blended with materials with greater packing discrepancies [H17 and H71], the distribution changes. Trend 3 is also apparent here, as when H47 is mixed with H17, a more efficient packer, its self-packing is decreased. The opposite is observed when H47 is mixed with H71: here it packs better. These trends are consistent with observations made with PRISM[22−24] for athermal mixtures, suggesting that many of these blends behave as if they are athermal. There are exceptions: H65 (Figure 11d) should pack better in H71 to follow this trend, but the opposite is observed. In the cases with exceptions [H71−H65 and H47−H65] there is an increased stabilization of A/B correlations at the expense of self-correlations. This effect is addressed in detail below.

To assess trend 2—how packing efficiency affects the changes with mixing—one must look at the overall spread in $g(r)$ from each pure component to its mixtures. However, this spread is also influenced by trend 1. A material with midrange butene content, such as H47, samples environments that are closer in structure to itself (trend 1) than do materials at the extremes of butene content, H71 or H17. Thus, to assess trend 2, one must be careful to eliminate the effect of trend 1 from the comparison. One way to do this is to compare H17 with H30. H17 is the better packer and, thus following trend 2, should change less on mixing than H30. This may be seen clearly by comparing parts a and b of Figure 11. The effect of trend 1 would render the spread in H17 larger relative to H30 since H17 samples an environment more dissimilar than any available to H30 [H17 in H71]. Since the observed spread is smaller despite the predictions of trend 1 (that work the opposite way), we attribute the smaller spread in H17 to trend 2; i.e., H17 is a more efficient packer than H30. Another

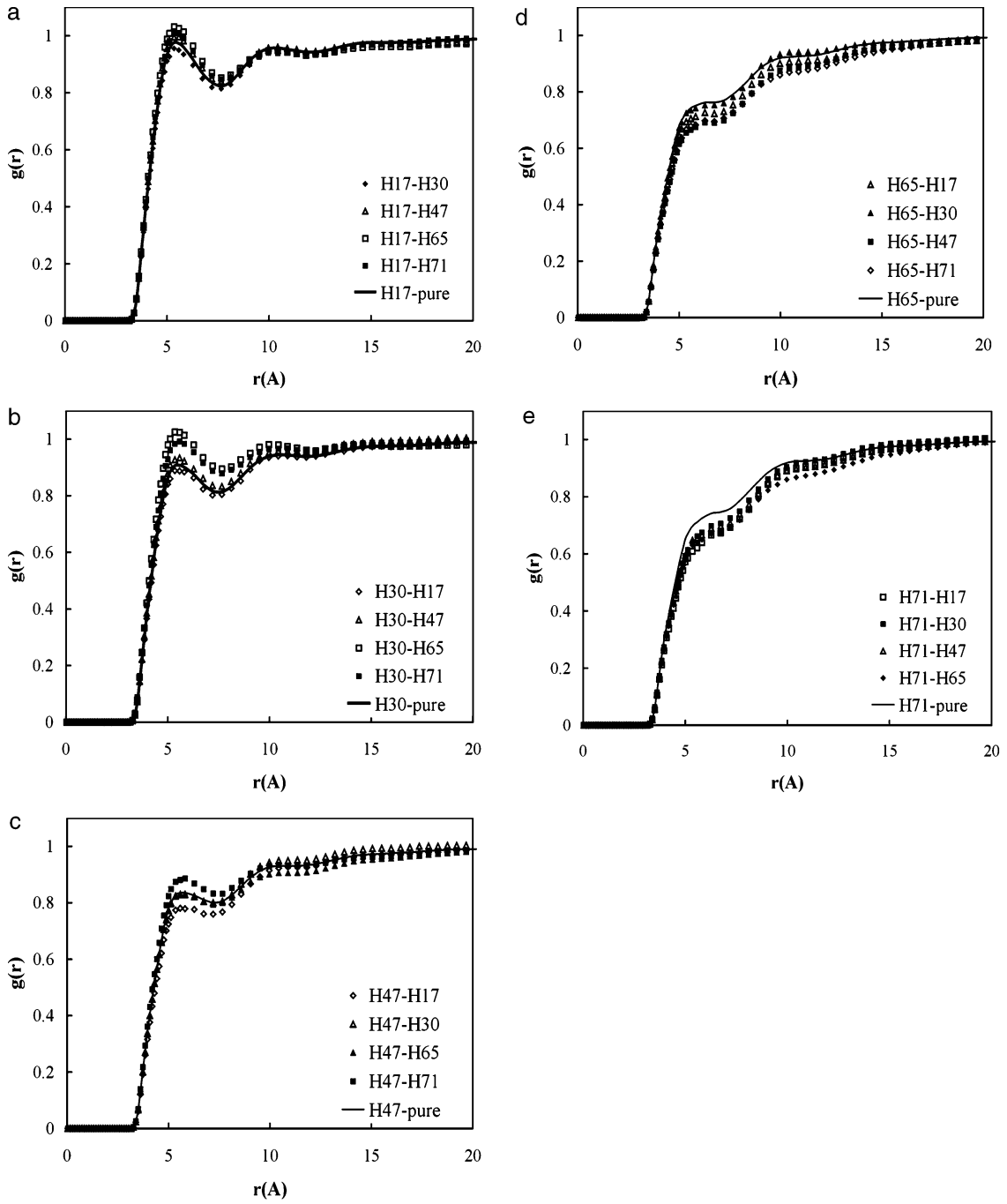

Figure 11. A/A intermolecular pair distribution function of EB copolymers as pure components and in different environments: (a) H17, (b) H30, (c) H47, (d) H65, (e) H71. Symbols are as in figure legend.

fair comparison is H17 with H71, since they cover the same range of environments. The spread in H71 is larger and extends over a greater spatial range than for H17.

Energetic vs Packing Effects. We now turn our attention to the reasons for the above observations. There are two possibilities: that the changes in mixtures occur because the system is able to lower its energy or that they occur because of entropy-driven packing effects. Most of our blends behave as if they are athermal in the sense that they follow the same general trends observed using PRISM[22−24] on athermal mixtures. The stiff component (in our case the more efficient packer) becomes more ordered, the flexible component (in our case the less efficient packer) becomes less ordered, and the cross distribution (A/B) is well described by an arithmetic or geometric mean. These trends are illustrated in Figure 12 for two blends: H71−H47 and H71−H30. All of the blends conform to this model with the exception of H71−H65 and H65−H47. This suggests that energetic effects have little to do with the observed behavior in these systems, despite the fact that the regular mixing formalism is applicable to all EB copolymer blends that have been tested so far.[9] Although this formalism appears to be energetically driven, the values of the solubility parameters ($=\Pi_{CED}^{1/2}$) are controlled by packing, as they scale directly with packing efficiency, i.e., the intermolecular pair distribution functions.

The behavior of the two blends that do not show athermal behavior is illustrated in Figure 13. Here there is a preference for A/B contacts at the expense of like

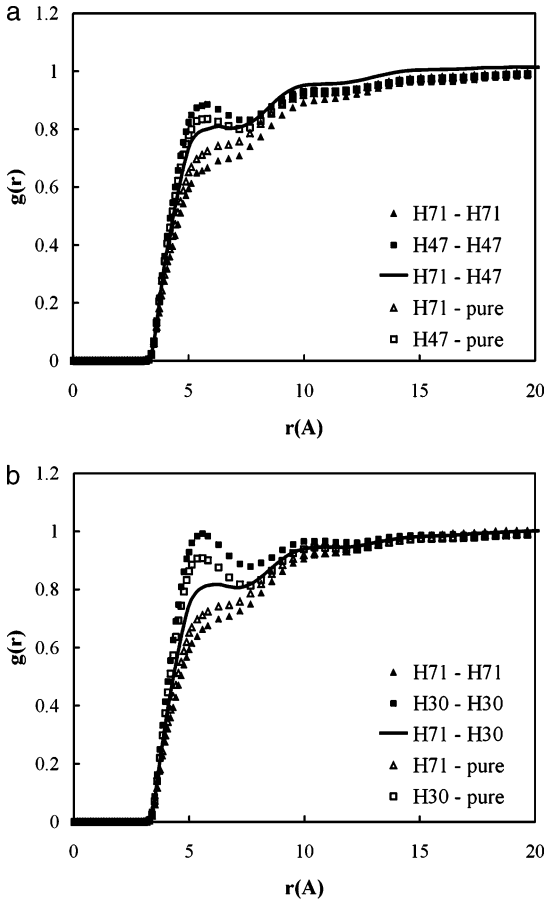

Figure 12. A/A, B/B, and A/B pair distribution functions in (a) H71−H17 and (b) H71−H30 mixtures compared with the pure component pair distribution functions. Symbols are as in figure legend.

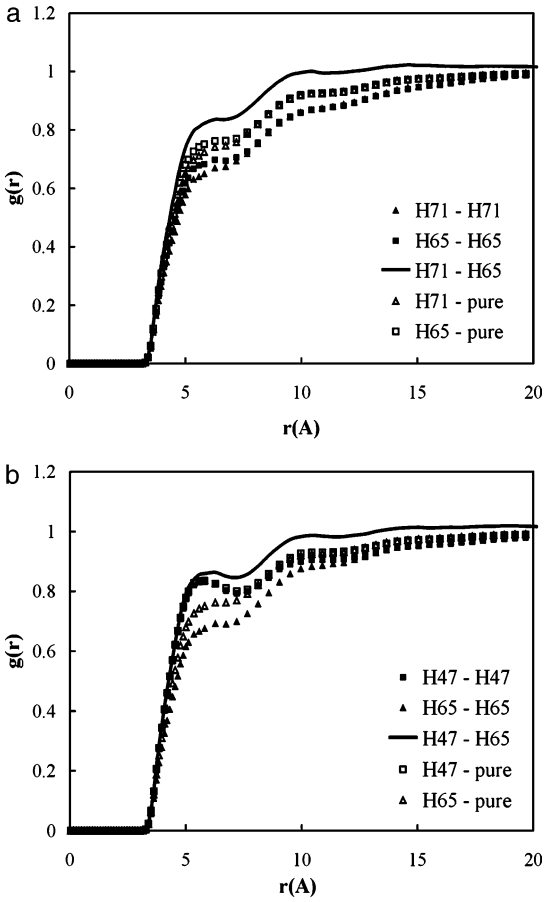

Figure 13. A/A, B/B, and A/B pair distribution functions in mixtures where A/B stabilization is observed: (a) H65−H71 and (b) H47−H65. Symbols are as in figure legend.

contacts, extending well past the R_g's of the components. The first issue to consider is whether this preference is driven by energetic considerations. If the formation of excess A/B contacts is driven by energetics, then the cohesive energy density of the blend should be greater than the average of the two components. The blend cohesive energy density and the average [$\Pi_{ave} = (\Pi_A\Pi_B)^{1/2}$] calculated from the pure components are shown in Table 5 for all mixtures involving H65. Recall that, for H65 with H71 and H47, A/B preference is observed, while for H65 with H30 and H17, it is not. It is seen that in all the cases the differences between the blend cohesive energy density and the average calculated from pure components are within statistical error. We have also calculated energies of mixing, and the resulting values are all zero within the error in their assignment. There is not a significant difference between those systems with the A/B stabilization and those where it is not observed. These results imply that the A/B stabilization is not a result of energetic preferences, suggesting that the stabilization is a packing effect. Both of these exceptions have been studied experimentally and follow regular mixing. Blends of H65 with H30 and H17 have not been the subject of experiment.

To assess packing-induced stabilization, we propose that the blend components have similar probabilities for ethylene and/or butene sequences of size *n*. These sequences are shown in Figure 14 for H65−H71 and H65−H17 blends. The sequences were determined as described for Table 4. The former system, which has A/B

Table 5. Blend Cohesive Energy Density and the Average [$\Pi_{ave} = (\Pi_A\Pi_B)^{1/2}$] Calculated from the Pure Components for All Mixtures Involving H65[a]

mixture	CED	Π_{ave}	mixture	CED	Π_{ave}
H65	203		H30−H65	214	214
H71−H65	196	199	H17−H65	217	218
H47−H65	205	208			

[a] The standard deviation in CED and Π_{ave} is ±2 MPa.

stabilization, shows a "match" between probabilities of ethylene A/ethylene B and butene A/butene B sequence distributions, in contrast with the H65−H17 blend. Thus, it is plausible that favorable A/B contacts arise from the availability of similarly matched sequence distributions in H65−H71 that are absent from H65−H17. Both H65−H47 and H65−H71 are consistent with the solubility parameter formalism,[41] as are the H17−H30 and H30−H47 mixtures. The remaining mixtures were either not considered or are immiscible. The latter two behave more like the examples in Figure 12, as opposed to Figure 13. For regular mixing to be applicable, one would expect that the self-distributions (A/A and B/B) would be close to those of the respective pure components and that the cross distribution (A/B) would follow an average. This is the case for H30−H47 (not shown), but for the two mixtures in Figure 13, it appears there is a cancellation of effects between the cross-distribution being enhanced and the self-distributions being suppressed. The H17−H30 blend has behavior intermediate between the two. We will consider regular mixing issues among these blends as well as blends of homopolymers in a forthcoming publication.

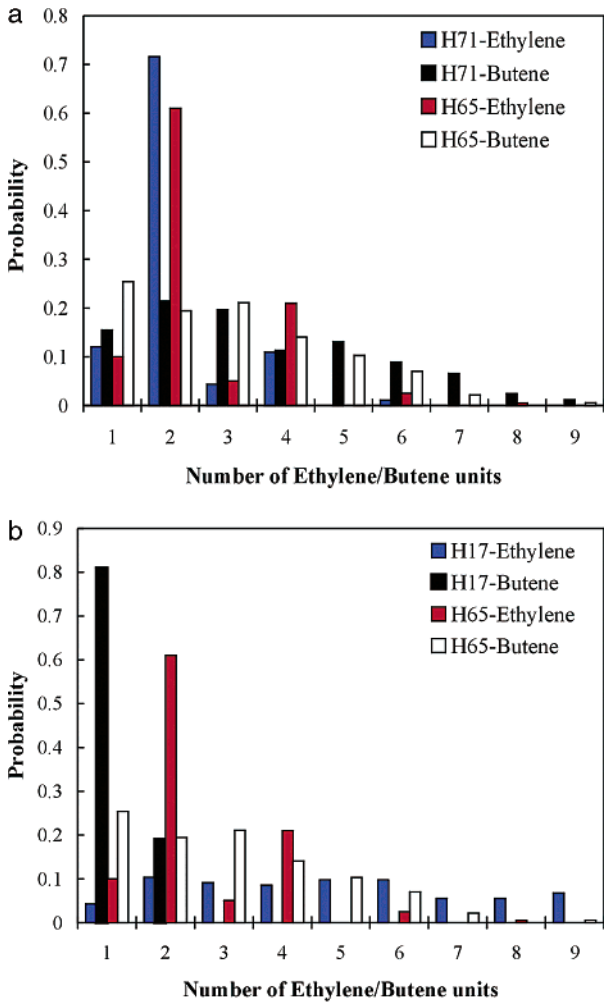

Figure 14. Probabilities of occurrence ethylene and butene units in mixtures: (a) H65−H71 and (b) H65−H17. Symbols are as in figure legend.

VI. Concluding Remarks

We have considered intermolecular packing in a series of random ethylene−butene copolymers. This packing varies with butene content in a systematic way. More importantly, we have investigated the changes in A/A or self-packing when these materials are placed in mixtures. In most cases the behavior of self- and cross (A/B)-packing follows the trends observed for athermal mixtures using PRISM. The implication is that purely energetic consequences of mixing are small in these systems. There are two exceptions in which there is a large enhancement of cross-correlations at the expense of self-correlations. These two exceptions have both been characterized experimentally as "regular" mixtures in that the Flory χ parameter may be expressed in terms of pure component solubility parameters.[9] In these systems, the blend cohesive energy density is lower than the average of the constituent components, suggesting that there is no energetic benefit from the substantial rearrangements of intermolecular packing. At this point, we do not have a clear understanding of the origin of the enhanced A/B correlations, although we have observed a match in the sequence distributions of the two components, not present in systems without the enhanced correlations, that could be a contributing factor.

Acknowledgment. Support of the National Science Foundation, Polymers Program via a CAREER Grant, DMR-0134910, is gratefully acknowledged.

References and Notes

(1) Maranas, J. K.; Kumar, S. K.; Debenedetti, P. G.; Graessley, W. W.; Mondello, M.; Grest, G. S. *Macromolecules* **1998**, *31*, 6998−7002.
(2) Maranas, J. K.; Kumar, S. K.; Debenedetti, P. G.; Graessley, W. W.; Mondello, M.; Grest, G. S. *Macromolecules* **1998**, *31*, 6991−6997.
(3) Luettmer-Strathmann, J. *J. Chem. Phys.* **2000**, *112*, 5473−5479.
(4) Balsara, N. P.; Fetters, L. J.; Hadjichristidis, N.; Lohse, D. J.; Han, C. C.; Graessley, W. W.; Krishnamoorti, R. *Macromolecules* **1992**, *25*, 6137−6147.
(5) Krishnamoorti, R.; Graessley, W. W.; Balsara, N. P.; Lohse, D. J. *J. Chem. Phys.* **1994**, *100*, 3894−3904.
(6) Krishnamoorti, R.; Graessley, W. W.; Balsara, N. P.; Lohse, D. J. *Macromolecules* **1994**, *27*, 3073−3081.
(7) Krishnamoorti, R.; Graessley, W. W.; Balsara, N. P.; Fetters, L. J.; Lohse, D. J.; Schulz, D.; Sissano, J. A.; Butera, R. J. *Macromolecules* **1994**, *27*, 3896−3901.
(8) Fetters, J. J.; Graessley, W. W.; Krishnamoorti, R.; Lohse, D. J. *Macromolecules* **1997**, *30*, 4973−4977.
(9) Graessley, W. W.; Krishnamoorti, R.; Reichart, G. C.; Balsara, N. P.; Fetters, L. J.; Lohse, D. J. *Macromolecules* **1995**, *28*, 1260−1270.
(10) Graessley, W. W.; Krishnamoorti, R.; Balsara, N. P.; Lohse, D. J. *Macromolecules* **1993**, *26*, 1137−1143.
(11) Maranas, J. K.; Kumar, S. K.; Debenedetti, P. G.; Graessley, W. W.; Mondello, M.; Grest, G. S. *Comput. Chem. Eng.* **1998**, *22*, S19−S26.
(12) Uhlherr, A.; Doxastakis, M.; Mavrantzas, V. G.; Theodorou, D. N.; Leak, S. J.; Adam, N. E.; Nyberg, P. E. *Europhys. Lett.* **2002**, *57*, 506−511.
(13) Kacker, N.; Weinhold, J. D.; Kumar, S. K. *J. Chem. Soc., Faraday Trans.* **1995**, *91*, 2457−2464.
(14) Han, J.; Boyd, R. H. *Macromolecules* **1994**, *27*, 5365−5370.
(15) Boyd, R. H.; Pant, P. V. K. *Macromolecules* **1991**, *24*, 6325−6331.
(16) Pant, P. V. K.; Han, J.; Smith, G. D.; Boyd, R. H. *J. Chem. Phys.* **1993**, *99*, 597−604.
(17) Curro, J. G.; Weinhold, J. D.; Rajasekaran, J. J.; Habenschuss, A.; Londono, J. D.; Honeycutt, J. D. *Macromolecules* **1997**, *30*, 6264−6273.
(18) Curro, J. G.; Webb, E. B., III; Grest, G. S.; Weinhold, J. D.; Putz, M.; McCoy, J. D. *J. Chem. Phys.* **1999**, *111*, 9073−9081.
(19) Weinhold, J. D.; Curro, J. G.; Habenschuss, A.; Londono, J. D. *Macromolecules* **1999**, *32*, 7276−7288.
(20) Schweizer, K. S.; Curro, J. G. *Adv. Polym. Sci.* **1994**, *116*, 319−377.
(21) Rajasekaran, J. J.; Curro, J. G. *J. Chem. Soc., Faraday Trans.* **1995**, *91*, 2427−2433.
(22) Stevenson, C. S.; Curro, J. G.; McCoy, J. D.; Plimpton, S. J. *J. Chem. Phys.* **1995**, *103*, 1208−1215.
(23) Singh, C.; Schweizer, K. S. *J. Chem. Phys.* **1995**, *103*, 5814−5832.
(24) Weinhold, J. D.; Kumar, S. K.; Singh, C.; Schweizer, K. S. *J. Chem. Phys.* **1995**, *103*, 9460−9474.
(25) Singh, C.; Schweizer, K. S.; Yethiraj, A. *J. Chem. Phys.* **1995**, *102*, 2187−2208.
(26) Singh, C.; Schweizer, K. S. *Macromolecules* **1997**, *30*, 1490−1508.
(27) Schweizer, K. S.; Singh, C. *Macromolecules* **1995**, *28*, 2063−2080.
(28) Akten, E. D.; Mattice, W. L. *Macromolecules* **2001**, *34*, 3389−3395.
(29) Clancy, T. C.; Putz, M.; Weinhold, J. D.; Curro, J. G.; Mattice, W. L. *Macromolecules* **2000**, *33*, 9452−9463.
(30) Rajasekaran, J. J.; Curro, J. G.; Honeycutt, J. D. *Macromolecules* **1995**, *28*, 6843−6853.
(31) Krishnamoorti, R. Ph.D. Dissertation, Princeton University, 1994.
(32) Jorgenson, W. L.; Madura, J. D.; Swenson, C. J. *J. Am. Chem. Soc.* **1984**, *106*, 6638−6646.
(33) Mondello, M.; Yang, H. J.; Furuya, H.; Roe, R. J. *Macromolecules* **1994**, *27*, 3566−3574.

(34) Berendsen, H. J. C.; Postma, J. P. M.; Van Gunsteren, W. F.; Di Nola, A.; Haak, J. R. *J. Chem. Phys.* **1984**, *81*, 3684−3690.
(35) Krishnamoorti, R. Ph.D. Thesis, Princeton University, 1994.
(36) Indrakanti, A.; Maranas, J. K.; Kumar, S. K. *Macromolecules* **2000**, *33*, 8865−8869.
(37) Paul, W.; Smith, G. D.; Yoon, D. Y. *Macromolecules* **1997**, *30*, 7772−7780.
(38) Smith, G. D.; Yoon, D. Y.; Zhu, W.; Ediger, M. D. *Macromolecules* **1994**, *27*, 5563−5569.
(39) Brown, D.; Clarke, H. R.; Okuda, M.; Yamazaki, T. *J. Chem. Phys.* **1994**, *100*, 1684−1692.
(40) Singh, C.; Schweizer, K. S. *J. Chem. Phys.* **1995**, *103*, 5814−5832.
(41) Graessley, W. W.; Krishnamoorti, R.; Reichart, G. C.; Balsara, N. P.; Fetters, L. J.; Lohse, D. J. *Macromolecules* **1995**, *28*, 1260−1270.

MA0210729